

Iterative Cluster Harvesting for Wafer Map Defect Patterns

Alina Pleli*, Simon Baeuerle*, Michel Janus, Jonas Barth, Ralf Mikut, Hendrik P. A. Lensch

Abstract—Unsupervised clustering of wafer map defect patterns is challenging because the appearance of certain defect patterns varies significantly. This includes changing shape, location, density, and rotation of the defect area on the wafer. We present a harvesting approach, which can cluster even challenging defect patterns of wafer maps well. Our approach makes use of a well-known, three-step procedure: feature extraction, dimension reduction, and clustering. The novelty in our approach lies in repeating dimensionality reduction and clustering iteratively while filtering out one cluster per iteration according to its silhouette score. This method leads to an improvement of clustering performance in general and is especially useful for difficult defect patterns. The low computational effort allows for a quick assessment of large datasets and can be used to support manual labeling efforts. We benchmark against related approaches from the literature and show improved results on a real-world industrial dataset.

Index Terms—Iterative clustering, silhouette score, unsupervised, wafer map defects

I. INTRODUCTION

SEMICONDUCTOR manufacturing is a fast-growing branch of industry, which is necessary to further advance developments, e.g. in the field of automotive electrification and many other applications. Worldwide, the demand for powerful and complex semiconductor chips is increasing. Individual processing steps are precisely controlled and errors should be detected as quickly and reliably as possible. Because of the large number of chips produced in a manufacturing facility, an automated error recognition is needed and can be supported by machine learning. Positions and types of defects found at different production steps of individual chips on a wafer can be displayed as an image, which is called wafer map. Clustering these wafer map images based on the type(s) of observed defect patterns should help to identify relevant defect patterns on the wafer maps. These patterns offer insights that can be used for root-cause analysis of defects. For example, if there is a line at certain points on the wafer, a device may have scratched the wafer during a production step.

The semiconductor manufacturing process is highly complex and variable. New defects can constantly occur where labeled data is not available and even for known defect patterns, labeling is a time-intensive task requiring expert knowledge.

A. Pleli and Hendrik P. A. Lensch are with the department of Computer Graphics, University of Tuebingen, D-72076 Tuebingen, Germany. (e-mail: alina.pleli@de.bosch.com) (*Alina Pleli and Simon Baeuerle are co-first authors.) (corresponding author: S. Baeuerle.)

S. Baeuerle and R. Mikut are with the Institute for Automation and Applied Informatics (IAI), Karlsruhe Institute of Technology (KIT), D-76344 Eggenstein-Leopoldshafen, Germany.

A. Pleli, S. Baeuerle, M. Janus and J. Barth are with the Robert Bosch GmbH, D-72762 Reutlingen, Germany.

Many other approaches have been published to classify defect patterns. This includes classical supervised approaches [1], transfer learning approaches using neural networks with similarity search [2], [3] and novel approaches using autoencoders [4], [5]. These usually require extensive and well-tuned training of the network architecture. In addition, for supervised classification training the set of error patterns must be specified beforehand and it relies on precise labeling.

We present an unsupervised machine-learning approach that does not require expert knowledge, is flexible for new, unknown defect patterns while at the same time simplifying the training setup. Our approach relies on iteratively removing clusters from the dataset based on the silhouette score [6] and redefining the feature space to maximize the separation between wafer-defect patterns in each iteration. This approach enables fast clustering on high-dimensional image data by feature extraction and dimensionality reduction. Our approach further alleviates the information loss inherent in these procedures by iteratively removing clusters and redefining the feature space. Additionally, the method filters out some defect patterns from the dataset, which are not noticeable in other clustering approaches, unless you apply methods like noise clustering.

We investigate the performance of our method using a real-world industrial wafer map dataset with expert labels for well-known recurring defect patterns and compare it against state-of-the-art methods. On this dataset we show that more homogeneous clusters are formed in comparison to a non-iterative procedure.

In Section II related approaches are presented to frame the proposed method in the area of conceptually and computationally similar methods. The methodology of our proposed approach is described in detail in Section III, and the method setup and data sets used are introduced in Section IV. With this, the results are presented and discussed in Section V-Section VII.

II. RELATED WORK

Guêrin et al. [7] analyzed a two-step approach to cluster images. They used a convolutional neural network (CNN) as feature extractor followed by a clustering algorithm and analyzed different combinations of both. They found that a combination of an Xception [8] feature extractor works well with agglomerative clustering (AC) [9], [10]. Napoletano et al. [11] investigated a three-step method with the application to images of nanofibrous materials. They use a ResNet-18 CNN as feature extractor together with a principal component analysis (PCA) and a k-means clustering.

A variety of methods has been explored to perform clustering iteratively. An iterative Gaussian mixture model (GMM) clustering approach for scene images has been introduced by Doan et al. [12], where the weights of the original dataset are iteratively computed. In this work, real scenes were evaluated along semantic axes (e.g., degree of naturalness of a scene, degree of verticality, and degree of openness). Compared to Doan et al. the feature extraction in our method is interchangeable and modular. The extractor should not be specified on the dataset (generic) and feature extraction should be done separately from the dimensional reduction.

Shorewala [13] extend the k-means algorithm. They drop samples with a distance larger than two standard deviations to the cluster mean from their assigned cluster and collect those as outliers within a separate group. Ma [14] proposed an extension of the Density-Based Spatial Clustering of Applications with Noise (DBSCAN) clustering method with regard to clusters of different sample densities. Lin et al. [15] developed a general iterative clustering approach via improving the proximity matrix and clusters of a base random forest. These iterative clustering methods [13]–[15] were however not yet applied to image datasets.

Intarapanich et al. [16] introduce an algorithm to cluster subpopulations in genotypic data. They iteratively apply a combination of PCA and fuzzy c-means clustering [17] to the dataset. With each iteration the dataset is split into two subsets until a stopping criterion is reached. They argue, that this procedure can resolve subpopulations better, especially if the samples of some subpopulations share a common region in PCA space while other subpopulations are located further away. This approach has been enhanced multiple times [18]–[22]. Those modifications include e.g. a modified stopping criterion [18], [20] or the assignment of individuals to an outlier group if they form a cluster with very few members [22]. These iterative approaches are all studied genotypic data. Odong et al. [23] use a PCA in combination with a clustering algorithm on genotypic data without iterations and report good results as compared to directly performing clustering on raw data.

The silhouette score [6] computes the similarity of a point to its own cluster compared to other clusters and is mainly used to determine the number of clusters and generally to compare different cluster results [24], [25]. Nidheesh et al. [26] utilized the silhouette score to cluster genomic data for cancer subtype discovery in a hierarchical bottom-up procedure. To the best of our knowledge, the silhouette score has not yet been used to automate iterative clustering.

Clustering on wafer maps has been heavily studied in recent years. Thus, different methods have been investigated for clustering wafer maps. Besides classical or variational autoencoders (AEs) [4], [5], [27], or Dirichlet process mixture model (DPMM) [28], classical clustering methods such as DBSCAN [29] are also explored. Additionally, hierarchical clustering methods (HCM) have been explored for clustering wafer maps. HCM start with each data point as its own cluster and iteratively try to combine the two most similar clusters into one. Zhang et al. [30] detected abnormal patterns via extracting of a small number of features by using sparse regression. These

features are used for a complete-link hierarchical clustering. Lee et al. [31] propose a similarity ranking method based on the Dirichlet process Gaussian mixture model (DPGMM) with HCM-based on symmetric Kullback-Leibler divergence (SKLD). The similarity ranking is conducted via the Jensen-Shannon divergence. Wang et al. [32] combine fuzzy c-means (FCM) with hierarchical linkage, Santos et al. [33] used average linkage and Tulala et al. [34] the Ward’s minimum variance criterion. For similarity search the Hamming distance was used [1], [35], Yu et al. ranked top-N wafer map defect patterns via Euclidean distance [36] and Hsu et al. employed weighted and modified Hausdorff distance [37]. Similar to Guêrin et al., Wang et al. use a pre-trained CNN to extract features from image data, which are then clustered by k-means [3]. Some other approaches with transfer learning are proposed [38], [39].

Unsupervised methods are helpful to retrieve similar defect patterns from large unlabeled datasets. However they are still outperformed in terms of accuracy by supervised methods, because an unsupervised method is not optimized on this metric in contrast to a supervised method. We introduce an iterative approach, which improves clustering performance as compared to its non-iterative counterpart.

III. METHODOLOGY

We propose an iterative approach based on a three-step clustering process consisting of feature extraction and variance-based dimensionality reduction before clustering. By iteratively removing (or "harvesting") wafer maps already partitioned into good clusters and repeatedly reinitializing the variance-based dimensionality reduction on the shrinking dataset, the expectation is that variances in the feature space, that were not captured during the one-time application of the three-step procedure (one-time clustering or OTC), can be separated in successive iterations. We name this method **Iterative Cluster Harvesting (ICH)**.

In the following we use a pre-trained CNN for feature extraction, principal component analysis (PCA) as a well-known dimensionality reduction, which ranks features based on their variances in the given dataset, and Agglomerative Clustering (AC) to define the clusters in each iteration. However, we will show that the benefits of our iterative approach remain, even if one of the component methods in the three-step process is swapped out based on preference or expectation of better one-time performance for a given dataset.

In the following, we describe the procedure of our harvesting method step-by-step, analogous to the presented process flow shown in Figure 1.

A. Three-step clustering

The core and start of the process flow is the aforementioned three-step clustering method. In the following, we describe each step separately, as it is also used in one-time clustering, before describing the ICH procedure and the changes in performance resulting from it.

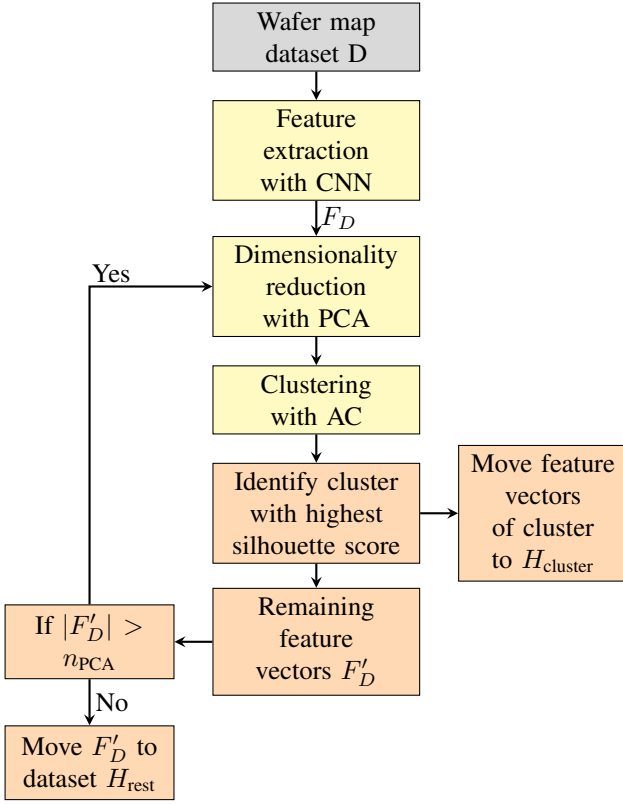


Figure 1. Iterative cluster harvesting scheme: CNN feature vectors F_D are extracted for the dataset D of wafer maps, and are processed with a dimensional reduction (PCA in our case) and clustered (using AC in our case). Per iterative run, the cluster with the highest value for the silhouette score is removed from F_D . Therefore in the subsequent iteration, the variances in the remaining dataset will lead to changes in the definitions of the PCA components. This allows our method to further separate the remaining dataset and find more homogeneous clusters over successive iterations.

1) *Feature extraction*: The first step of the process flow is feature extraction with a CNN for the wafer map dataset D . For unsupervised clustering of images, the use of features from a pre-trained CNN is useful as this provides an abstract representation of images [40]. In this paper, the choice of CNN architectures for feature extraction is not analyzed and interested readers are referred to [7], [41], where extensive experiments were conducted to identify the optimal feature extractor for different datasets. Thus, visually recognizable components of a wafer map are detected and can now be represented with a feature vector $f_i \in F_D$.

2) *Dimensionality reduction*: After the feature vectors are computed, the number of dimensions is still large enough to slow down and prohibit clustering from finding semantically relevant features. We reduce this high number of dimensions further by performing a principal component analysis (PCA) [42] to identify the features responsible for the largest variances in the dataset. It retains important and removes irrelevant dimensions. In this way, computational costs can be reduced significantly. For this method there is one freely selectable parameter: the number of principal components (n_{PCA}). The choice of this parameter can be dataset-dependent and problem-specific.

The dimensional reduction method itself is only one com-

ponent within the clustering method of the proposed ICH approach in this paper and is not the focus of this study. For a mathematical description see [42], [43]. We use the implementation of PCA from the Python package scikit-learn [44].

3) *Clustering*: Clustering of the resulting PCA feature space is conducted as a next step with the agglomerative clustering (AC) method. The algorithm is a hierarchical clustering algorithm in which each data point is considered as one cluster [45]. From bottom to the top the clusters are agglomerated with Euclidean distance and the Ward’s linkage. These are the default parameters of the scikit-learn [44] implementation of the AC method. As a hyperparameter the number of expected clusters has to be determined. For a detailed description and comparison of the different methods see [46].

A detailed investigation and optimization of the hyperparameters of the individual building blocks of the three-step clustering approach is not the objective of this work. Here, we also use the implementation of scikit-learn [44].

B. Harvesting clusters with silhouette score

As shown in Figure 1, after the three steps of feature extraction, dimension reduction and clustering, the clusters are now sorted to determine the most suitable cluster to be harvested in the iteration. For this purpose, the silhouette score is calculated for each data point [6]:

$$s_{i,j} = \frac{b - a}{\max(a, b)} \quad (1)$$

with the mean distance a between a data point j and all other points in the cluster c_i and the mean distance b between a sample j and all other data points in the next nearest cluster to c_i . In this way the silhouette score $s_{i,j}$ indicates how close one data point is to the other data points in its cluster c_i in the PCA feature space and simultaneously calculates the distance to the next nearest cluster to it.

For each cluster c_i , we calculate the silhouette score s_i as the mean of all $s_{i,j}$ for the included data points j . Thus, with this formula in Equation 1, dense clusters which are far away from other clusters are scored highly. Possible values for the silhouette score s_i range from -1 to 1 , with an optimum value of 1 .

After calculating s_i for all clusters we identify cluster $c_{s_{max}}$ with the maximum silhouette score value

$$s_{max} = \max_i s_i. \quad (2)$$

This cluster has the highest separability compared to the rest of the dataset and at the same time a high similarity of wafer maps within the cluster.

Consequently, the feature vectors $F_D \in c_{s_{max}}$ are moved to a dataset $H_{cluster}$. Thus, one cluster is harvested to dataset $H_{cluster}$ per iteration based on the maximum of the silhouette scores in the specific iteration, and only the remaining CNN feature vectors F'_D are used for the next iteration.

The sub-process of PCA and AC is then repeated, always harvesting one cluster in each iteration. As already mentioned, the PCA and the subsequent AC can be dominated at the start

by the variance in the full data caused by individual samples and clusters whose feature vectors are very different from the rest of the dataset. Therefore the key aspect of our method is to successively remove data points from the dataset D and repeat PCA and AC on the new dataset to successively focus on finer variances in the dataset.

This process is repeated until there are not enough wafer maps left in the dataset to sensibly perform a PCA. In our experiments we found if $|F'_D| > n_{\text{PCA}}$ to be a good rule-of-thumb for a stopping criterion.

Note that, when the stopping criterion is fulfilled, some feature vectors F'_D , which were never included in any dense and highly separated cluster, will remain unclustered. This dataset of feature vectors we denote as H_{rest} .

C. Summary and extensions of method

To summarize we restate the main features of our harvesting method: after the one-time feature extraction by a CNN, the dimension reduction and clustering is performed iteratively, harvesting per iteration the cluster with the highest s_i in the PCA space during this iteration, thereby reducing the variance of the remaining dataset. Thus, at the end of iterative process, we have sorted most of the data points from the original dataset D into clusters in the dataset H_{cluster} , while separating out a dataset H_{rest} of intricate wafer maps.

1) *Refining H_{cluster} based on size:* During our studies we found it useful to further refine H_{cluster} . For our use case it is relevant that clusters are large enough. For example, if there is a cluster that contains less than 5 wafer maps, the significance of this defect pattern for root-cause analysis can be questioned. So the clusters in H_{cluster} are filtered by their size to a dataset H_{small} and only large enough clusters are kept in H_{cluster} . The number of required wafer maps n_{min} in a cluster can be adjusted depending on the underlying use case and the user's own definition of what is the minimum size of a cluster. Such a filtering based on cluster size has been used in a similar fashion on genotypic data by Chaichoompu et al. [22].

2) *Full assignment of wafer maps to H_{cluster} :* Both due to the existence of H_{rest} and the extension that creates H_{small} , not all wafer maps in D are included in the result dataset H_{cluster} . Although separating noise clusters and small clusters can be useful, it might be desirable to assign all wafer maps to clusters, either for performance comparisons or for practical considerations. For this purpose we propose the simple method of assigning the feature vectors in H_{rest} and H_{small} to clusters in H_{cluster} by a nearest neighbor assignment. Note that the nearest neighbor search is done in the CNN feature vector space, and not in the PCA space, where components and therefore distances might change iteration by iteration. We consider this final assignment as optional, although it allows each wafer map to be assigned to a cluster while preventing the number of resulting clusters from becoming too large and having very few wafer maps in some clusters.

3) *Free Parameters of the full method:* In the presented ICH method, there are certain hyperparameters that can be adjusted depending on the data set and the use case. In principle

the CNN network architecture, dimensionality-reduction and clustering methods as well as the distance metric for silhouette scores can be exchanged, depending on the type of dataset. The parameters to be freely chosen for this method are the number of principal components allowed (n_{PCA}), the number of clusters allowed per iteration (n_c) and the minimum number above which a formed cluster is considered large enough (n_{min}). We motivate each selection for our experiments in Section IV-A.

D. Evaluation metric

To evaluate our results we use homogeneity as the performance metric. As the term implies, homogeneity is a measure of the purity of the clusters formed. A cluster is considered pure if it contains only one defect class and no mixtures of different defect classes. The value for this metric h is between 0 and 1 and is calculated by the formula

$$h = 1 - \frac{H(C|K)}{H(C)} \in [0, 1] \quad (3)$$

while

$$H(C|K) = - \sum_{c=1}^C \sum_{k=1}^K \frac{n_{c,k}}{n} \cdot \log \left(\frac{n_{c,k}}{n_k} \right) \quad (4)$$

and

$$H(C) = - \sum_{c=1}^C \frac{n_c}{n} \cdot \log \left(\frac{n_c}{n} \right) \quad (5)$$

with H denoting the entropy, C the set of classes and K the set of clusters, n the total number of samples, n_c and n_k the number of samples respectively belonging to class c and cluster k and finally $n_{c,k}$ the number of samples from class c assigned to cluster k . If an optimally pure clustering succeeds, in which only clusters with one class each are found, i.e. the entropy $H(C|K)$ is zero, the homogeneity approaches the value 1. The conditional entropy of the class distribution can be used to determine how close the proposed clustering is to the optimally homogeneous division of the data, i.e. each cluster consisting only of members of one class. The metric value becomes smaller the more members of different classes are found in the clusters. $H(C|K)$ is maximal and equal to $H(C)$ "if the clustering does not provide any new information" [47]. The homogeneity becomes $h = 0$ in this case. We used the implementation of the scikit-learn collection [44]. The homogeneity metric is used for evaluation in this work because it uses the labels as a basis. Since we are examining a labeled dataset, homogeneity is a valid measure of the purity of the true labels in the clustering result.

With the homogeneity described, our experiments are evaluated. Before presenting the results, the following section describes the specific configuration of our method and the datasets used for our experiments.

IV. EXPERIMENTAL SETUP

A. Method setup

To perform our ICH method, a selection of methods for the three-step method is required and the associated parameters

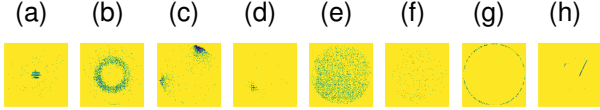


Figure 2. Exemplary images of wafer maps in the dataset WM1K with (a) Center, (b) Donut, (c) Edge-Loc, (d) Loc, (e) Near-Full, (f) Random, (g) Ring and (h) Scratch defect pattern.

Table I
CHARACTERISTICS OF USED WAFER MAP DATASETS WITH DEFECT-TYPE DISTRIBUTION

Dataset	WM1K	WM811K_sub
Resolution	200×200	$27 \times 27 \pm 2$
Total number	1302	923
Center	166	150
Donut	208	9
Edge-Loc	208	150
Loc	120	150
Near-Full	150	53
Random	150	141
Ring	150	120
Scratch	150	150

must be set. We use the Xception architecture as a feature extractor, with weights pre-trained on the ImageNet dataset as available within Keras [48]. Specifically, we use the outputs of the MaxPooling2D layer *block13_pool*, which has been identified to work well in the two-step procedure analyzed by Guérin et al. [7]. For each wafer map with a resolution of $(299, 299)$ and three channels an array with dimensions $(10, 10, 1024)$ is generated. The array is flattened to a feature vector with 102,400 dimensions.

As dimensionality reduction method we use PCA. In our experiments, we found that a number of $n_{PCA} = 20$ PCA dimensions is a reasonable choice. These first 20 components cover about 80% of the variance in the full dataset.

For the clustering method we use AC. We set the number of clusters within an individual iteration to $n_c = 15$. Allowing fewer clusters for ICH may result in mixed clusters with different true labels, once the unique clusters with characteristic salient properties are removed from the dataset to be clustered. Therefore, care must be taken to ensure that the number of allowed clusters for AC is large enough. If the value is chosen larger, small clusters can be found and the resulting number of result clusters may become larger, which is not the purpose of a clustering method.

To identify the cluster that is filtered out during an iteration, the cosine distance was used as the distance metric for the silhouette score.

As mentioned before, we filter $H_{cluster}$ for a minimum size of at least $n_{min} = 5$ wafer maps per cluster. In order to quote results for a full assignment of all wafer maps, the final nearest-neighbor assignment is conducted, both for the H_{rest} and H_{small} cluster sets.

B. Dataset description

The proposed clustering method is evaluated using two wafer map datasets, which are sharing the same logic for the

defect classes. The main evaluation in this paper is shown by using a real-world wafer map dataset WM1K provided by a semiconductor manufacturing company. WM1K contains 1302 wafer maps belonging to the following eight defect patterns: Center, Donut, Edge-Loc, Loc, Near-Full, Random, Ring or Scratch. Examples of these defect patterns are shown in Figure 2. The labels were assigned manually by domain experts. The variance of the appearances of defect distributions may vary for different defect patterns. For example, the visual appearance of the defect distribution for Center, Donut, and Near-Full classes are quite uniform due to their geometry and class definition. A Donut can vary in diameter and thickness, but the characteristic shape stays the same. On the other hand, the Edge-Loc and Scratch defects in particular can occur at very different locations with various orientations on the wafer maps. Ring defects can be putatively evaluated as a simple class. However, the Ring can also only occur as a circular segment. Near-Full and Random defects vary in density of defects. Even in areas where two wafer maps of these types are both affected by defects, the distribution of defects appears randomly, so the pixel-based variations may be large. These differences will have a significant impact on clustering performance, as discussed later in Section V. The number of wafer maps in WM1K varies between 120 and just over 208 for all defect classes, but no class is severely underrepresented, which can be seen in Table I. The wafer maps have a resolution of $(200, 200)$ pixels. To match the input resolution of the pre-trained CNN the wafer maps are resized to $(299, 299)$ and copied along a newly introduced third dimension. Besides rescaling, no further preprocessing is applied to WM1K. The method is evaluated on the not-preprocessed wafer maps, as the aim of this paper is to investigate to what extent defect patterns can be clustered, partly containing many randomly occurring defects that do not belong to the raw, typical signature of the defect class.

The second dataset used for evaluating the method is a subset of the public dataset WM811K [36]. WM811K contains a wide variety of different image resolutions. Furthermore, classes are heavily imbalanced for many resolutions. Therefore, we carry out the major part of our analysis on the dataset WM1K, which is much better maintained and allows direct statements based on a real-world use case. To prove that our method is generally applicable, we carry out an additional evaluation on the public WM811K dataset. We extract images with a resolution around $(27, 27)$. To mitigate the current class imbalance, we consider up to 150 images per defect pattern (see Table I). We denote this subset of the public dataset as WM811K_sub. The same pre-processing as before is performed to match the standard CNN input resolution.

V. RESULTS

This section presents the performance of our proposed cluster harvesting method mainly on the dataset WM1K as described in Section IV-B. First we report the overall performance of our ICH approach and show the improvement compared with one-time clustering with the same algorithm sequence.

To give further insight into the procedure, we show the workings on the first iteration in detail and follow the clustering progress through to the final iteration. We also present examples of the clusters filtered out by our additional filter on the cluster size, to illustrate our reasoning behind this choice. To illustrate the limitations of performance on the given dataset, we show a detailed view on the types of clusters which still show strong mixing of true defect types.

To further demonstrate the competitiveness of our iterative method, we also show a benchmark comparison by total homogeneity with other one-time clustering approaches. We validate that the performance improvement from our iterative approach is stable with regards to the choice of method for each part of the three-step sequence, by presenting an ablation study, where we quote results with a viable alternative algorithm chosen for each part.

Finally, we show how our proposed harvesting method improves clustering performance on the public dataset WM811K_sub as well.

A. Results of iterative cluster harvesting

Applying our method described in Section III to the WM1K wafer map dataset automatically determines the number of clusters, yielding 57 clusters. The homogeneity for this clustering result is $h = 0.90$ and with optional full assignment $h = 0.86$.

As a first, and most instructive comparison with the proposed method, we apply the three-step procedure only once (OTC). Our proposed ICH approach shows significantly improved performance compared with the OTC approach on the WM1K dataset both for partial and full assignment. This comparison, together with the other performance comparisons described in the following are summarized in Table II. With OTC on WM1K (full assignment) some defect classes are well clustered and some are mixed with others. This method yields a homogeneity metric value of $h = 0.77$ (full assignment) and $h = 0.82$ (partial assignment). This already shows the utility of the filtering introduced by ICH, as it identifies the subset of the dataset that is easier to cluster and removes many outliers and small aggregations of wafer maps which are otherwise wrongly assigned in OTC.

To understand the class-wise improvement of performance we present the confusion matrix, normalized by true labels in Figure 3, where the predicted labels are taken to be the majority class true label within a given cluster. For the defect patterns Center, Donut, Loc, and Ring, OTC results in a percentage of correctly clustered wafer maps range from 92% to 100% (see Figure 3a). For the other defect patterns (Edge-Loc, Near-Full, Random, and Scratch), the majority class makes up for 57% – 75% of the cluster. These defect patterns could not be distinguished well from each other by the OTC method, resulting in clusters that contain wafer maps with different defect patterns. For example, Edge-Loc and Loc is mixed, Near-Full is mixed with Edge-Loc, Random is mixed with Donut and Scratch is mainly mixed with Loc. The number of clusters formed for each defect pattern is listed at the top of the confusion matrix in Figure 3a. In particular, many clusters

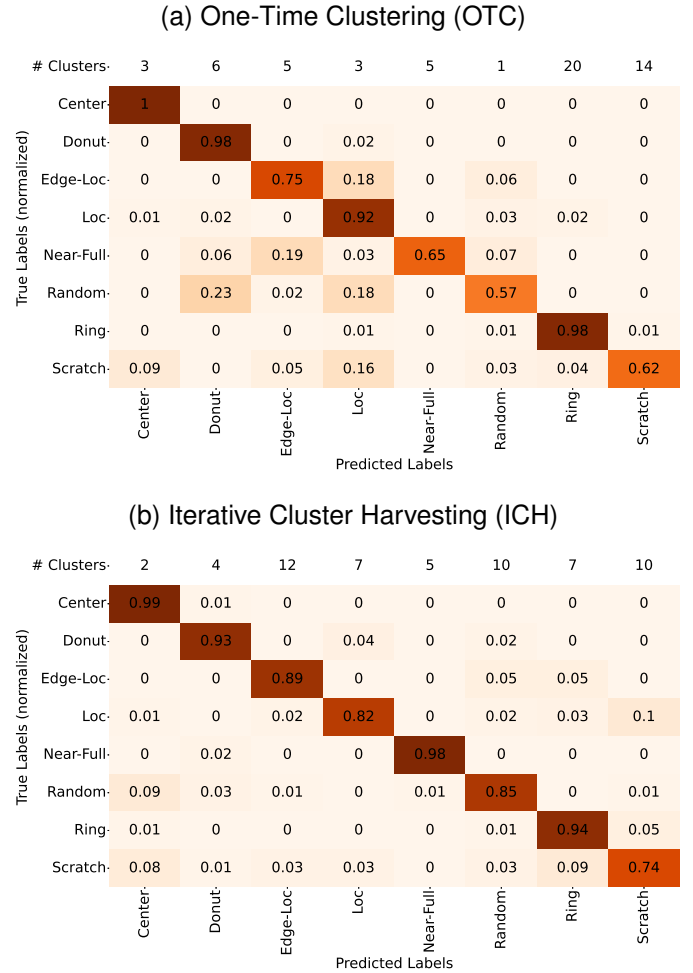


Figure 3. Confusion matrices of OTC (a) and ICH (b) approach with full assignment of WM1K dataset. For each cluster, the predominant true label is evaluated and assigned as the predicted label. If there are other true labels in a predominant cluster of a particular true label, this can be read along the vertical column of the true label. Values are normalized to the number of data points of the true labels. Since there are usually multiple clusters for the same label, they are combined in order to calculate the confusion matrix. The number of individual clusters per true label is shown in the top row of the respective confusion matrix.

were formed for Ring and Scratch (20 and 14, respectively) and only one cluster for defect pattern Random.

To evaluate the change in performance for the individual defect patterns for OTC and ICH, we consider the diagonal entries of the confusion matrices in Figure 3. Our proposed harvesting procedure improves the diagonal percentages considerably for the four defect patterns that had low values with OTC procedure. Comparatively small decreases are seen for the four defect patterns which had very high values with the OTC procedure. This overall reduction of off-diagonal entries as well as the changes in the number of clusters per majority class, illustrates how the iterative harvesting of individual, well-separated clusters prevents lumping many different true labels together, sometimes at the expense of creating more, smaller clusters.

B. Illustration of iterative cluster harvesting process

To demonstrate the way of harvesting, the PCA space of the first iteration is presented in Figure 4. It shows the seven leading PCA components, color-coded by the true label.

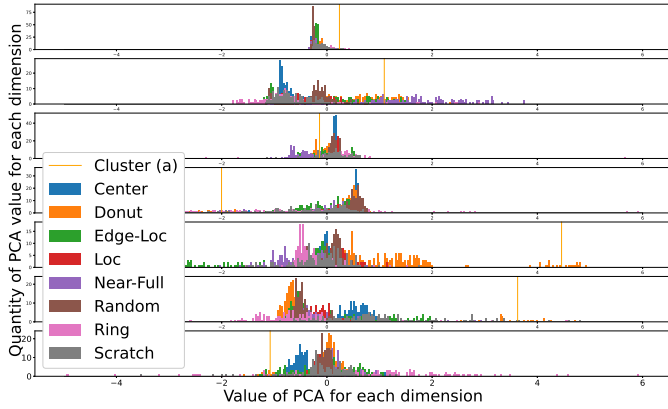


Figure 4. Histogram over the feature values of the first seven principal components after applying the OTC to WM1K, which is equal to the first iteration of the ICH procedure. Colors are assigned according to the true labels. Mean values of an exemplary cluster (a) shown in Figure 5a are marked in each principal component.

Although this illustration shows only projections into the first several PCA dimensions (not the silhouette score actually used to measure the separation between clusters), it already becomes apparent how some groupings of very well separated wafer maps can be identified. Looking at the color-coding of these groupings, we find large, well-separated groups for the classes we expect to have a very characteristic appearance from the discussion in Section IV-B. Other classes with varying appearance such as Loc or Random largely share a common range of values. Some clusters are well separated from the remaining samples. For the cluster with the highest silhouette score after performing the first iteration of our ICH procedure, we have marked the mean values within the different PCA dimensions. While its individual sample values are still dispersed, its distance to the neighboring samples is especially large in the principal components 4, 5, and 6. This visually distinct cluster contains 22 Donut wafer maps. The mean image of this cluster is shown in Figure 5a. Note that the mean images are calculated by summing all

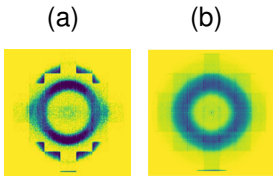


Figure 5. (a): Mean image of the Donut cluster identified in the 1st iteration by ICH for WM1K and (b): mean image of all wafer maps of WM1K from the Donut class except for the wafer maps from the identified cluster (a).

of wafer maps pixel by pixel and dividing by the number of images in the cluster. Visually it is apparent why this cluster is well separated, as there is a significant difference from the mean image of the Donut class without these clustered wafer maps, as the stepped edges around the wafer maps only appear in the wafer maps in Figure 5a.

After the first iteration the wafer maps in this cluster are extracted to H_{cluster} , which leads

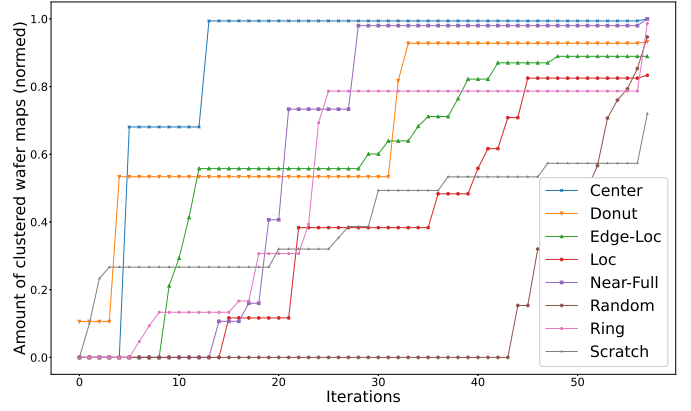


Figure 6. Number of clustered wafer maps (normalized to 1) as a function of iterations for each defect class for ICH on the WM1K dataset. Per iteration, the dominating true label for the resulting cluster is determined and counted. The wrongly assigned wafer maps in the cluster are not counted. The last iteration relates to the nearest neighbor assignment, which is performed for the wafer maps in H_{rest} and H_{small} .

to an initial assignment of about 10% of wafer maps from the Donut class. The consecutive accumulation of correctly assigned wafer maps per defect class is shown in Figure 6. Along the x -axis of Figure 6, one can follow which majority class is being harvested in the cluster for each iteration, while small clusters are not considered and are assigned in the last iteration at the end in Figure 6. It can be seen that often there are consecutive iterations where the majority class of the harvested clusters is the same, suggesting that the PCA evolves slowly in these cases, keeping focus on the features relevant for this class. Switches of majority defect class (i.e. one line flattening out and another rising) denote iterations where the variance in the dataset is then dominated by another class, potentially causing larger changes in the PCA dimensions. By this logic a loose ranking by variance of the different classes can be extracted from this figure. Defect patterns with a rather uniform visual appearance such as Center or Donut form clusters which exhibit high silhouette scores and are extracted from D during early iterations. Defect patterns with varying appearance such as Scratch or Random are clustered at later iterations. Looking at the second-to-last iteration in Figure 6 one sees the total, correctly assigned fraction of wafer maps from each class after ICH but before the final nearest-neighbor assignment. Before nearest-neighbor assignment almost all defect classes have a fraction of ≈ 0.75 of their wafer maps assigned correctly, with the Scratch class being the only exception with a fraction of about 0.6 during the regular ICH procedure.

Figure 6 further shows the performance of the final assignment of our approach, where the remaining samples (H_{rest} and H_{small}) are assigned to their nearest neighbors of already assigned samples in the CNN feature space. After nearest neighbor assignment, all correctly assigned fractions increase, showing the validity of the simple approach. It is also interesting to note that especially the two classes with the lowest fractions, Scratch and Ring, rise dramatically in the final assignment. This suggests that these maps lie close-by

Cluster	Dominating TL	Mixed TL
A	 Loc	 Donut
B	 Ring	 Edge-Loc
C	 Random	 Donut

Figure 8. Exemplary wafer maps of clusters with mixed true labels (TL) after applying ICH to the WM1K dataset.

in feature space to well-separated clusters with this majority class, but many samples are scattered too widely to be included in well-separated clusters during the main ICH procedure.

C. Examples of wafer maps from H_{small}

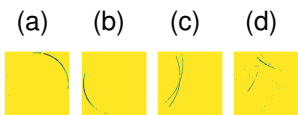


Figure 7. Exemplary images of wafer maps identified by ICH with high purity and small number in WM1K. Images (a-b) show Ring and (c-d) Scratch wafer maps.

To illustrate what types of wafer maps we remove during iterations which formed a small cluster (less than 5 wafer maps) we show some examples in Figure 7. As can be seen in this figure, these wafer maps display very distinct patterns and often near zero pixel-wise variance inside the small

clusters. While potentially interesting to diagnose small aberrations in the wafer manufacturing, they are less valuable than the larger clusters found in other iterations, which point to production problems that affect a larger population of wafers potentially over extended time periods.

D. Examples of clusters with low homogeneity

As a result of the ICH process, many clusters have been created that are strongly dominated by one defect class (high homogeneity). However, even with this ICH approach some mixed clusters remain. A visual assessment as shown in Figure 8 gives a deeper insight into the cause for the wrong assignments: some samples share a similar visual appearance, even though they are assigned with different labels. For example, cluster A in Figure 8 is composed of Loc defect patterns located in the upper left wafer area. The Donut defect pattern mixed into this Loc cluster looks very similar, with defects mainly present in the upper left wafer area as well. A highly similar visual appearance although with different true labels is further shown for the exemplary clusters B and C.

E. Comparison with other one-time clustering methods

To illustrate the competitiveness of ICH, we also quote homogeneity numbers for some other relevant one-time clustering methods in Table II. To enable a direct comparison, we

Table II
BENCHMARK OF OUR PROPOSED ICH APPROACH ON WM1K DATASET WITH 57 CLUSTERS. THE HOMOGENEITY VALUES ARE REPORTED WITHOUT ASSIGNMENT OF WAFER MAPS IN H_{REST} AND H_{SMALL} (PARTIAL ASSIGNMENT) AND WITH ASSIGNMENT OF ALL WAFER MAPS (FULL ASSIGNMENT).

Method	Partial assignment	Full assignment
OTC	0.82	0.77
CNN + AC [7]	0.87	0.78
PCA + AC	0.73	0.74
Var-AE + AC [34]	0.72	0.73
ICH (ours)	0.90	0.86

use the same number of clusters as the number of clusters identified during our ICH approach for the benchmarking methods. The choice of hyperparameters (e.g., CNN network architecture, PCA dimensions) remained the same for each component.

Applying the method presented by Guérin et al. [7] (CNN+AC) on the full dataset WM1K (full assignment), we see that the homogeneity decreases to $h = 0.78$ compared to $h = 0.86$ (ICH). The performance of this two-step procedure is almost equal to the one of the OTC (CNN+PCA+AC), which yields a homogeneity of $h = 0.77$. If PCA is applied directly to the images without feature extraction by a CNN, the homogeneity of the clustering result decreases to $h = 0.74$. Similar to Tulala et al. [34], we also train a variational autoencoder on the wafer map dataset. It is trained for 40 epochs and the latent space with 20 dimensions is clustered using AC. This results in a smaller homogeneity of $h = 0.73$.

The same applies for the results of the part of wafer maps that were divided into sufficiently large clusters by ICH (partial assignment). The clustering result of ICH has the highest homogeneity with $h = 0.86$, while CNN+AC performing better than OTC.

The proposed cluster harvesting procedure ICH exhibits a competitive performance when compared to other methods which are similar in terms of setup effort and computational complexity.

F. Ablation Study

Table III
ABLATION STUDY: RELATIVE IMPROVEMENT Δ_{REL} OF HOMOGENEITY METRIC (ICH VS OTC) FOR DIFFERENT CHOICES OF FEATURE EXTRACTORS (FEAT. EXTR.), DIMENSIONAL REDUCTION (DIM. RED.) AND CLUSTERING METHODS FOR WM1K WITH FULL ASSIGNMENT.

Ablation Factor	Exemplary Pipeline	OTC	ICH	Δ_{rel}
Proposed Pipeline	Xception + PCA + AC	0.77	0.86	12 %
Feat. Extr.	ResNet + PCA + AC	0.75	0.82	9 %
	VGG16 + PCA + AC	0.74	0.80	8 %
Dim. Red.	Xception + ISOMAP + AC	0.78	0.81	4 %
	Xception + SVD + AC	0.60	0.68	13 %
Clustering	Xception + PCA + GMM	0.74	0.80	8 %
	Xception + PCA + k-means	0.73	0.80	10 %

In order to investigate whether the ICH process provides an improvement in homogeneity independent of the choice of the

Table IV

BENCHMARK OF OUR PROPOSED ICH APPROACH ON WM811K_SUB WITH 66 CLUSTERS. THE HOMOGENEITY VALUES ARE REPORTED WITHOUT ASSIGNMENT OF WAFER MAPS IN H_{REST} AND H_{SMALL} (PARTIAL ASSIGNMENT) AND WITH ASSIGNMENT OF ALL WAFER MAPS (FULL ASSIGNMENT)..

Method	Partial assignment	Full assignment
OTC	0.75	0.67
CNN + AC [7]	0.77	0.69
PCA + AC	0.68	0.64
Var-AE + AC [34]	0.56	0.52
ICH (ours)	0.80	0.62

underlying network architecture, the dimensionality reduction and the clustering procedure, an ablation study was conducted on the full WM1K dataset using the nearest neighbor assignment. One component of the three-step process is changed at a time and the comparison of homogeneity between the OTC and ICH execution of the process is evaluated (see Table III).

When the network architecture is changed, the relative improvement due to the iterations ranges from 8% to 9%. If one exchanges the dimensionality reduction to either ISOMAP or SVD, homogeneity is also improved by applying our proposed ICH approach. When changing the clustering method to GMM an improvement by the iterative procedure of 8% and with k-means of 10% is seen, compared with the 12% improvement when applying ICH with AC clustering.

G. Results of ICH on WM811K_sub

Applying our method described in Section III to the WM811K_sub wafer map dataset automatically determines the number of clusters, yielding 66 clusters. The homogeneity for this clustering result is $h = 0.80$ for the clusters in H_{cluster} of ICH (see also Table IV). The application of OTC leads to a homogeneity of $h = 0.75$.

Therefore our proposed ICH approach significantly improves performance over the OTC approach on the dataset of clusters selected by ICH (6% relative improvement). ICH outperformed the other benchmark methods as well. Using the optional variant with full assignment and forcing all data points from small filtered out clusters to a cluster via nearest neighbor assignment, the homogeneity for the WM811K_sub dataset drops to $h = 0.62$. For this dataset, about 20% of the wafer maps end up in H_{small} and the assignment via nearest neighbor search leads to a sharp drop in cluster performance. Therefore it is not surprising that on the entire dataset other methods lead to a slightly higher homogeneity. OTC achieves $h = 0.67$ and CNN+AC performs best with $h = 0.69$.

We note however that omitting the difficult wafer maps, identified by our method in H_{rest} and H_{small} , the clustering performance of all methods improves noticeably. For example, comparing the homogeneity values of the OTC with the data from H_{cluster} and the full assignment, the homogeneity improves strongly from $h = 0.67$ to $h = 0.75$. Thus, the utility of our method as a filter to create a well-clusterable sub-dataset can also be clearly shown when applied to the WM811K_sub dataset.

VI. DISCUSSION

We have shown that our method of iteratively performing variance-based dimensionality reduction and removing sets of wafer maps, that are well-separated, leads to improvements in homogeneity of clustering results in comparison with competitive non-iterative approaches. We note however that for the Var-AE the comparison on our dataset might not be fully conclusive, as we would expect an improved performance of the auto-encoder with a larger dataset size. Nonetheless we still claim an advantage in simplicity and training effort of our method in comparison to Var-AE or similar methods.

We have also shown that these benefits persist also when replacing individual components of the preferred pipeline of methods. After applying a modular feature extraction method, which is appropriate for images, our method can be applied with competitive speed and performance to the clustering of image datasets, again with freedom of choice for the clustering method without suffering usual difficulties from dealing with high-dimensional image data. Our iterative method does not introduce new free hyperparameters, apart from the stopping criterion for the minimal number of samples and the optional filter criterion on the size of the selected clusters. We note however that the number of PCA dimensions as well as the expected number of clusters for AC, which are also parameters of OTC, have a strong influence on the performance of our method and their meaning is slightly changed (e.g. number of clusters per AC iteration does not define the total number of clusters found by ICH).

As an extension of the method, refinement of the collected clusters based on size provides a set of difficult, or "noise" wafer maps. In clustering, such data points lead to the formation of many small clusters and with a fixed number of resulting clusters, as is common in clustering approaches, fewer clusters are available for the remaining data points. Therefore, we consider the automated identification of difficult samples as an advantage of our approach, but provide a simple method to assign these wafer maps automatically at the end of the core method to achieve a full assignment. Instead of executing this final assignment, the filtered sub-dataset can be used for manual review of these difficult wafer maps.

We showed the benefit of using our method as a filter, as we obtain much better homogeneity when applying some of the other considered clustering methods (namely OTC and CNN+AC) on our filtered dataset compared with the full dataset. For the other benchmark methods (PCA+AC and Var-AE+AC), there is little impact on cluster performance whether one clusters with or without the difficult wafer maps. It seems that direct PCA on image vectors as well as Var-AE training are robust against removal of these small sets of difficult wafer maps.

Although overall performance of ICH is very competitive, we still observe some strongly mixed clusters in our main dataset under study (WM1K). We have shown examples of these cases to illustrate that we believe these cases to be difficult to judge even for humans, without additional information about the root-cause of the defect patterns. Thus our method could even be used in these cases to trigger manual review of dataset

labels and to identify overlaps or borderline cases. For the WM811K_sub dataset, the homogeneity value with full assignment is lower for ICH than for the other methods studied (with exception of Var-AE). We showed in our results that the main cause for this are a large number of small clusters, which are formed during ICH and then not assigned by the core method but by nearest-neighbor assignment. This is not surprising, but rather indicates that this subset from the public dataset WM811K contains many wafer maps that are difficult to cluster. As with the WM1K dataset, filtering out the difficult wafer maps in WM811K_sub improves clustering performance in the benchmark methods. Nonetheless, we recommend examining the filtered-out data and adjusting the minimum value of an allowed cluster size in cases where an excessive amount of data points is filtered out during the application of ICH.

In summary, we conclude that our iterative method is applicable for a wide range of feature extraction and clustering methods. Apart from configuring the hyperparameters, we did not make any specific adaptations to the algorithm in order to improve its performance on wafer map images. So, we expect it to be easily adaptable to other use cases and data types. Considering our original use case of wafer map defect patterns, our method is well suited when combined with the filtering options discussed above. In combination with example visualizations as shown in our paper, manual and interactive evaluation of the results should be possible. In this way, we expect it to be of great use in supporting defect engineers in detecting both rare and recurring defect patterns and providing them a narrowly focused starting point for root-cause analysis. Finally, we expect that the proposed ICH method could be used in conjunction with or as a stand-in for supervised image classification methods. While by itself it would perform slightly worse in terms of clustering homogeneity, it would be useful for example to reduce the manual effort for labeling. Our method could also play a valuable part when a trade-off between performance and training effort can be considered, especially for datasets where the required domain knowledge is scarce.

VII. CONCLUSION

Our proposed ICH approach improves the performance of unsupervised clustering wafer maps strongly. This performance improvement results from the potentially easier clustering of small variances in the data set in the course of the iterative application of dimensionality reduction to the successively reduced dataset. In addition, our method helps to identify data points in a dataset that mainly lead to a worse clustering result because they are very different from the rest of the dataset and consist of only a small number of wafer maps.

This method is very well suited to support manual labeling or review of existing labels. The method was not specialized for the wafer map use case, allowing it to be easily transferred to use cases with other image data. No manual effort is required for the use of this method, except for the selection of hyperparameters. A separate investigation could examine how

this ICH method works with high-resolution images, i.e. when the resolution is larger than the required input dimension of the feature extractor. This is relevant, for example, for clustering scanning electron microscope (SEM) images of wafers, which are typically acquired at higher resolutions.

APPENDIX

AUTHOR STATEMENT

We describe the individual contributions of Alina Pleli (AP), Simon Baeuerle (SB), Michel Janus (MJ), Jonas Barth (JB), Ralf Mikut (RM) and Hendrik P. A. Lensch (HL) using CRediT [49]: *Writing - Original Draft*: AP; *Writing - Review & Editing*: AP, SB, MJ, JB, RM, HL; *Conceptualization*: AP, SB, MJ, JB, RM, HL; *Investigation*: AP, SB; *Methodology*: AP, SB; *Software*: AP, SB; *Supervision*: MJ, JB, RM, HL; *Project Administration*: MJ, HL; *Funding Acquisition*: MJ, JB, RM, HL.

REFERENCES

- [1] T. Nakazawa and D. V. Kulkarni, "Wafer map defect pattern classification and image retrieval using convolutional neural network," *IEEE Transactions on Semiconductor Manufacturing*, vol. 31, no. 2, pp. 309–314, 2018.
- [2] S. Cheon, H. Lee, C. O. Kim, and S. H. Lee, "Convolutional neural network for wafer surface defect classification and the detection of unknown defect class," *IEEE Transactions on Semiconductor Manufacturing*, vol. 32, no. 2, pp. 163–170, 2019.
- [3] S. Wang, S. Yan, Q. Shen, C. Luo, J. Ai, L. Li, D. Wang, S. Ding, and Q. Xia, "Wafer defect map similarity search using deep learning in semiconductor manufacturing," in *2021 China Semiconductor Technology International Conference (CSTIC)*, 2021, pp. 1–4.
- [4] T. Santos and R. Kern, "Understanding wafer patterns in semiconductor production with variational auto-encoders," in *Proc. 26th Eur. Symp. Artif. Neural Netw. Comput. Intell. Mach. Learn. (ESANN)*, Apr. 2018, pp. 141–146.
- [5] J. Hwang and H. Kim, "Variational deep clustering of wafer map patterns," *IEEE Transactions on Semiconductor Manufacturing*, vol. 33, no. 3, pp. 466–475, 2020.
- [6] P. J. Rousseeuw, "Silhouettes: A graphical aid to the interpretation and validation of cluster analysis," *Journal of Computational and Applied Mathematics*, vol. 20, pp. 53–65, 1987. [Online]. Available: <https://www.sciencedirect.com/science/article/pii/0377042787901257>
- [7] J. Guêrin, O. Gibaru, S. Thiery, and E. Nyiri, "CNN features are also great at unsupervised classification," arXiv:1707.01700, Tech. Rep., 2018. [Online]. Available: <https://arxiv.org/abs/1707.01700>
- [8] F. Chollet, "Xception: Deep learning with depthwise separable convolutions," in *2017 IEEE Conference on Computer Vision and Pattern Recognition (CVPR)*, 2017, pp. 1800–1807.
- [9] A. K. Jain and R. C. Dubes, *Algorithms for Clustering Data*. Prentice Hall, 1988.
- [10] N. Rajalingam and K. S. S. Ranjini, "Hierarchical clustering algorithm - a comparative study," *International Journal of Computer Applications*, vol. 19, pp. 42–46, 2011.
- [11] P. Napoletano, F. Piccoli, and R. Schettini, "Anomaly detection in nanofibrous materials by CNN-based self-similarity," *Sensors*, vol. 18, no. 1, 2018.
- [12] K. N. Doan, T. T. Do, and T. H. Le, "Scene image clustering based on boosting and GMM," in *Proceedings of the Second Symposium on Information and Communication Technology*, ser. SoICT '11. New York, NY, USA: Association for Computing Machinery, 2011, pp. 226–232. [Online]. Available: <https://doi.org/10.1145/2069216.2069258>
- [13] V. Shorewala, "Anomaly detection and improvement of clusters using enhanced k-means algorithm," in *2021 5th International Conference on Computer, Communication and Signal Processing (ICCCSP)*, 2021, pp. 115–121.
- [14] L. Ma, "An improved and heuristic-based iterative DBSCAN clustering algorithm," in *2021 IEEE 5th Advanced Information Technology, Electronic and Automation Control Conference (IAEAC)*, vol. 5, 2021, pp. 2709–2714.

- [15] Z. Lin, E. Laska, and C. Siegel, "A general iterative clustering algorithm," *Statistical Analysis and Data Mining: The ASA Data Science Journal*, 2022.
- [16] A. Intarapanich, P. J. Shaw, A. Assawamakin, P. Wangkumhang, C. Ngamphiw, K. Chaichoompu, J. Piriyaopongsa, and S. Tongshima, "Iterative pruning PCA improves resolution of highly structured populations," *BMC Bioinformatics*, vol. 10, no. 1, p. 382, Nov. 2009.
- [17] J. C. Bezdek, *Pattern recognition with fuzzy objective function algorithms*. New York, NY, USA: Plenum Press, 1981.
- [18] T. Limpiti, A. Intarapanich, A. Assawamakin, P. Wangkumhang, and S. Tongshima, "Iterative PCA for population structure analysis," in *2011 IEEE International Conference on Acoustics, Speech and Signal Processing (ICASSP)*, Prague, Czech Republic, May 2011, pp. 597–600.
- [19] T. Limpiti, A. Intarapanich, A. Assawamakin, P. J. Shaw, P. Wangkumhang, J. Piriyaopongsa, C. Ngamphiw, and S. Tongshima, "Study of large and highly stratified population datasets by combining iterative pruning principal component analysis and structure," *BMC Bioinformatics*, vol. 12, no. 1, p. 255, 2011.
- [20] T. Limpiti, C. Amornbunchornvej, A. Intarapanich, A. Assawamakin, and S. Tongshima, "iNJclust: iterative neighbor-joining tree clustering framework for inferring population structure," *IEEE/ACM Transactions on Computational Biology and Bioinformatics*, vol. 11, no. 5, pp. 903–914, 2014.
- [21] C. Amornbunchornvej, T. Limpiti, A. Assawamakin, A. Intarapanich, and S. Tongshima, "Improved iterative pruning principal component analysis with graph-theoretic hierarchical clustering," in *2012 9th International Conference on Electrical Engineering/Electronics, Computer, Telecommunications and Information Technology*, Phetchaburi, Thailand, May 2012, pp. 1–4.
- [22] K. Chaichoompu, F. A. Yazew, S. Tongshima, P. J. Shaw, A. Sakuntabhai, B. Cavadas, L. Pereira, and K. Van Steen, "A methodology for unsupervised clustering using iterative pruning to capture fine-scale structure," bioRxiv:234989v1, Tech. Rep., Jan. 2017. [Online]. Available: <http://biorxiv.org/content/early/2017/12/15/234989.abstract>
- [23] T. L. Odong, J. van Heerwaarden, T. J. L. van Hintum, F. A. van Eeuwijk, and J. Jansen, "Improving hierarchical clustering of genotypic data via Principal Component Analysis," *Crop Science*, vol. 53, no. 4, pp. 1546–1554, Jul. 2013.
- [24] K. R. Shahapure and C. Nicholas, "Cluster quality analysis using silhouette score," in *2020 IEEE 7th International Conference on Data Science and Advanced Analytics (DSAA)*, 2020, pp. 747–748.
- [25] A. Dudek, "Silhouette index as clustering evaluation tool," in *Classification and Data Analysis*, K. Jajuga, J. Batóg, and M. Waleśiak, Eds. Cham: Springer International Publishing, 2020, pp. 19–33.
- [26] N. Nidheesh, K. A. A. Nazeer, and P. M. Ameer, "A hierarchical clustering algorithm based on silhouette index for cancer subtype discovery from genomic data," *Neural Comput. and Applic.*, vol. 32, pp. 11 459–11 476, 2020.
- [27] C. Weber, A. Tripuramallu, P. Czerner, and M. Fathi, "Clustering wafer defect patterns within the semiconductor industry based on wafer maps, using an agile unsupervised deep learning approach," in *2021 IEEE International Conference on Systems, Man, and Cybernetics (SMC)*, 2021, pp. 1913–1918.
- [28] D. Kim and P. Kang, "Dynamic clustering for wafer map patterns using self-supervised learning on convolutional autoencoders," *IEEE Transactions on Semiconductor Manufacturing*, vol. 34, no. 4, pp. 444–454, 2021.
- [29] K. S.-M. Li, L. Li-Yang Chen, K. C.-C. Cheng, P. Yi-Yu Liao, S.-J. Wang, A. Y.-A. Huang, N. Tsai, L. Chou, G. C.-H. Han, J. E. Chen, H.-C. Liang, and C.-L. Hsu, "Automatic inspection for wafer defect pattern recognition with unsupervised clustering," in *2021 IEEE European Test Symposium (ETS)*, 2021, pp. 1–2.
- [30] W. Zhang, X. Li, S. Saxena, A. J. Strojwas, and R. A. Rutenbar, "Automatic clustering of wafer spatial signatures," *2013 50th ACM/EDAC/IEEE Design Automation Conference (DAC)*, pp. 1–6, 2013.
- [31] J. H. Lee, I.-C. Moon, and R. Oh, "Similarity search on wafer bin map through nonparametric and hierarchical clustering," *IEEE Transactions on Semiconductor Manufacturing*, vol. 34, no. 4, pp. 464–474, 2021.
- [32] C.-H. Wang, S.-J. Wang, and W.-D. Lee, "Automatic identification of spatial defect patterns for semiconductor manufacturing," *Int. J. Prod. Res.*, no. 23, pp. 15 169–5185, 2006.
- [33] T. Santos, S. Schrunner, B. C. Geiger, O. Pfeiler, A. Zernig, A. Kaestner, and R. Kern, "Feature extraction from analog wafermaps: A comparison of classical image processing and a deep generative model," *IEEE Transactions on Semiconductor Manufacturing*, vol. 32, no. 2, pp. 190–198, 2019.
- [34] P. Tulala, H. Mahyar, E. Ghalebi, and R. Grosu, "Unsupervised wafermap patterns clustering via variational autoencoders," in *2018 International Joint Conference on Neural Networks (IJCNN)*. IEEE, 2018, pp. 1–8. [Online]. Available: <https://ieeexplore.ieee.org/abstract/document/8489422/>
- [35] N. Yu, Q. Xu, and H. Wang, "Wafer defect pattern recognition and analysis based on convolutional neural network," *IEEE Transactions on Semiconductor Manufacturing*, vol. 32, no. 4, pp. 566–573, 2019.
- [36] M.-J. Wu, J.-S. R. Jang, and J.-L. Chen, "Wafer map failure pattern recognition and similarity ranking for large-scale data sets," *IEEE Transactions on Semiconductor Manufacturing*, vol. 28, no. 1, pp. 1–12, 2015.
- [37] C.-Y. Hsu, W.-J. Chen, and J.-C. Chien, "Similarity matching of wafer bin maps for manufacturing intelligence to empower industry 3.5 for semiconductor manufacturing," *Computers and Industrial Engineering*, vol. 142, p. 106358, 2020. [Online]. Available: <https://www.sciencedirect.com/science/article/pii/S0360835220300929>
- [38] P. Bhatnagar, T. Arora, and R. Chaujar, "Semiconductor wafer map defect classification using transfer learning," in *2022 IEEE Delhi Section Conference (DELCON)*, 2022, pp. 1–4.
- [39] Z. Shen and J. Yu, "Wafer map defect recognition based on deep transfer learning," in *2019 IEEE International Conference on Industrial Engineering and Engineering Management (IEEM)*, 2019, pp. 1568–1572.
- [40] J. Schmidhuber, "Deep learning in neural networks: an overview," *Neural networks : the official journal of the International Neural Network Society*, vol. 61, pp. 85–117, 2015.
- [41] J. Guérin, S. Thiery, E. Nyiri, O. Gibaru, and B. Boots, "Combining pretrained CNN feature extractors to enhance clustering of complex natural images," *Neurocomputing*, vol. 423, pp. 551–571, 2021. [Online]. Available: <https://doi.org/10.1016%2Fj.neucom.2020.10.068>
- [42] I. T. Jolliffe, *Principal Component Analysis*. New York, NY: Springer New York, 2002, pp. 1–9. [Online]. Available: https://doi.org/10.1007/0-387-22440-8_1
- [43] T. Hastie, R. Tibshirani, J. Friedman, and J. Franklin, "The elements of statistical learning: Data mining, inference, and prediction," *Math. Intell.*, vol. 27, pp. 83–85, 2004.
- [44] F. Pedregosa, G. Varoquaux, A. Gramfort, V. Michel, B. Thirion, O. Grisel, M. Blondel, P. Prettenhofer, R. Weiss, V. Dubourg, J. Vanderplas, A. Passos, D. Cournapeau, M. Brucher, M. Perrot, and E. Duchesnay, "Scikit-learn: Machine learning in Python," *Journal of Machine Learning Research*, vol. 12, pp. 2825–2830, 2011.
- [45] W. H. E. Day and H. Edelsbrunner, "Efficient algorithms for agglomerative hierarchical clustering methods," *Journal of Classification*, vol. 1, p. 7–24, 1987.
- [46] K. Sasirekha and P. Baby, "Agglomerative hierarchical clustering algorithm- a review," vol. 3, 2013.
- [47] A. Rosenberg and J. Hirschberg, "V-measure: A conditional entropy-based external cluster evaluation measure," in *Proceedings of the 2007 Joint Conference on Empirical Methods in Natural Language Processing and Computational Natural Language Learning*. Prague, Czech Republic: Association for Computational Linguistics, 2007, pp. 410–420. [Online]. Available: <https://aclanthology.org/D07-1043>
- [48] F. Chollet *et al.*, "Keras," <https://keras.io>, 2015.
- [49] A. Brand, L. Allen, M. Altman, M. Hlava, and J. Scott, "Beyond authorship: attribution, contribution, collaboration, and credit," *Learned Publishing*, vol. 28, no. 2, pp. 151–155, Apr. 2015. [Online]. Available: <http://doi.wiley.com/10.1087/20150211>